NANO LETTERS

pubs.acs.org/NanoLett Letter

Room-Temperature Hole Plasmons and Plasmon-Phonon Interactions in Epitaxial *p*-Type Scandium Nitride

Prasanna Das, Debmalya Mukhopadhyay, Emma R. Bartelsen, Renuka Karanje, Krishna Chand Maurya, Pavithra Rao, Ashalatha Indiradevi Kamalasanan Pillai, Shankar Kumar Selvaraja, Magnus Garbrecht, Joshua D. Caldwell, and Bivas Saha*

Cite This: *Nano Lett.* 2026, 26, 9614–9621 Read Online

ACCESS | Metrics & More | Article Recommendations | Supporting Information

ABSTRACT: The plasmon resonance represents collective oscillations of free electrons, enabling subwavelength light confinement and local field enhancement in conductive media. While electron-based plasmons in metals and *n*-type semiconductors have been widely explored, their hole-based counterparts in *p*-type semiconductors remain largely underexplored due to low hole densities and large effective masses that push plasmon response to the far-infrared with strong damping. Here, we present conclusive experimental evidence of low-loss, room-temperature hole plasmons in the mid-infrared regime, realized in epitaxial *p*-type scandium nitride thin films. Enabled by a high hole concentration of ~1.4 × 10^{20} cm^{-3} and mobility of ~21 cm^2 V^{-1} s^{-1}, these hole plasmons exhibit strong confinement with moderate damping. Furthermore, by tuning hole concentrations to spectrally overlap the plasmonic resonance with surface phonon polaritons, we demonstrate a mixed hole-plasmon−LO-phonon interaction giving rise to broadband hybrid absorption response. These results establish robust hole plasmonics in *p*-type semiconductors for infrared nanophotonic devices.

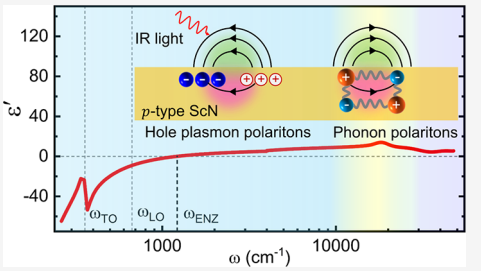

KEYWORDS: *Plasmonics, Hole plasmons, Surface phonon polaritons, Plasmon-phonon interactions, Scandium nitride (ScN)*

Nanoscale confinement of light through strong light-matter interactions is a cornerstone of modern nanophotonics.[1,2] Among the various strategies for achieving such subdiffractional optical confinement and extreme field enhancements, polaritons, the hybrid quasiparticles formed due to the coupling of photons with coherently oscillating dipoles, have emerged as one of the most versatile platforms.[3,4] Plasmon polaritons,[5,6] the collective oscillations of free electrons in conductive materials such as metals and doped *n*-type semiconductors,[7,8] have been studied extensively, with their resonances spanning the near-ultraviolet (UV) to far-infrared (IR) spectral range, and enabling transformative applications in sensing,[9,10] energy conversion,[11] telecommunications,[12] and super-resolution imaging.[13,14]

While electron-based plasmons have thus been studied across a wide spectral range, hole-based plasmons, representing collective excitations of holes in *p*-type semiconductors, remain comparatively less explored (Figure 1a). The larger effective mass and multiband valence-band structure of holes generally result in lower plasma frequencies and increased damping, placing hole plasmon resonances in the far-infrared to terahertz spectral range and making their experimental realization challenging.[15,16] While these characteristics are often viewed as limitations, requiring higher hole densities and offering reduced tunability, they also provide a distinct regime in which to examine the influence of carrier type, band structure, and scattering mechanisms on the plasmonic response. To date, such constraints have limited systematic exploration of hole-based plasmonics, particularly in the mid-infrared regime where experimental access and control are more readily achievable. Realizing robust hole plasmons in this spectral window, therefore, enables a platform to investigate carrier-dependent[17,18] plasmonic behavior and its interaction with lattice vibrations, with potential implications for infrared nanophotonics and optoelectronic device functionalities.

Beyond free-carrier excitations, phonon polaritons (PhPs), coherent oscillations of polar lattice vibrations strongly coupled with light offer a complementary and equally powerful approach to mid-to-far-infrared light-matter interactions (Figure 1a).[19,20] In a polar dielectric material, the real component of the dielectric permittivity (ε') undergoes a positive-to-negative transition at the longitudinal optic (LO) phonon frequency and exhibits a pole at the transverse optic (TO) phonon frequency, thereby, exhibiting negative values within the Reststrahlen band.[21] The interaction of light with optical phonons also enable surface PhP (SPhP) propagation

Received: May 20, 2026
Revised: July 8, 2026
Accepted: July 8, 2026
Published: July 16, 2026

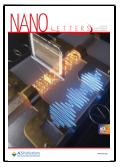

https://doi.org/10.1021/acs.nanolett.6c02445
Nano Lett. 2026, 26, 9614–9621

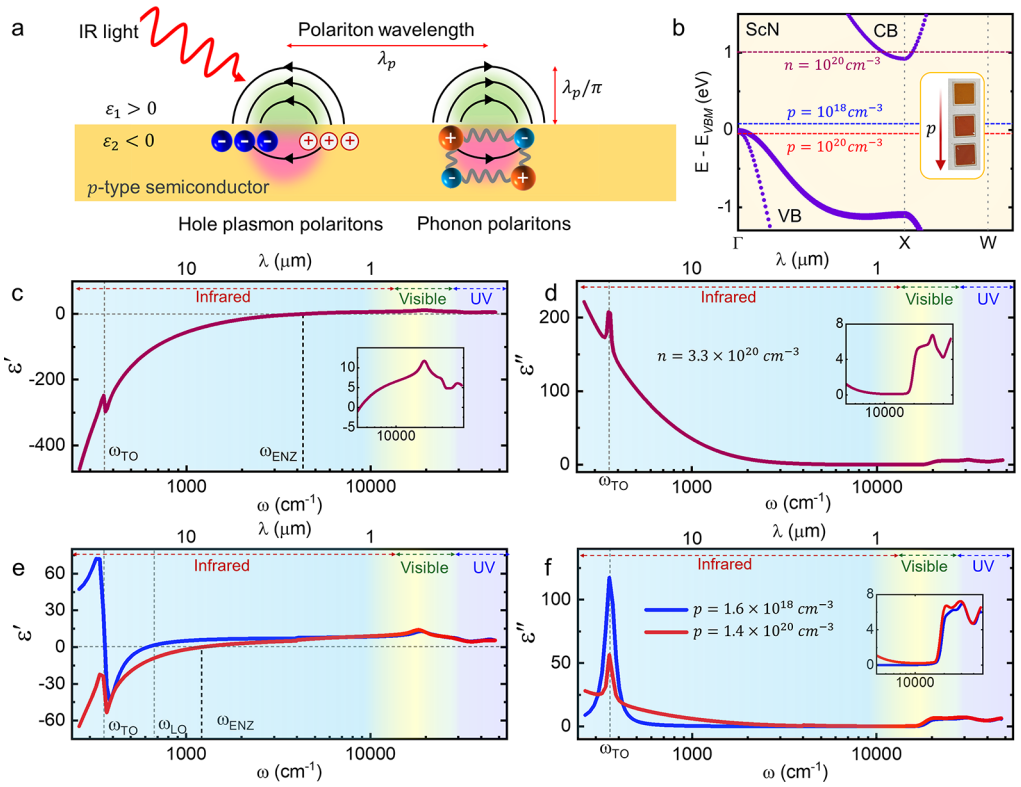

Figure 1. Hole plasmon resonance in *p*-type ScN. (a) Schematic illustration of hole plasmon and phonon polaritons in a *p*-type polar semiconductor. (b) Density functional theory calculated electronic band structure of ScN depicting the Fermi level positions corresponding to different carrier concentrations and carrier types. The inset highlights the color variation of ScN films with increasing Mg-hole concentration. Real and imaginary components of the dielectric permittivity of *n*-type (c and d) and *p*-type (e and f) ScN films across the near-UV to far-infrared spectral range. While *n*-type ScN exhibits a pronounced plasmonic response characterized by a positive-to-negative ε' crossover at 4250 cm^{-1} (2.35 μm), the low-doped *p*-type ScN shows predominantly phonon-polaritonic behavior characterized by the negative ε' values within the Reststrahlen band. The highly doped *p*-type ScN demonstrate an ENZ crossover at ∼1200 cm^{-1} (8.33 μm) representing its hole plasmonic behavior at room-temperature. The ε'' representing optical loss in *n*-type ScN increases in the mid-IR range due to the onset of plasmonic behavior and shows a peak at the TO phonon frequency. In contrast, the low-doped *p*-type ScN exhibits optical losses arising predominantly from phonon−polariton contributions. For the highly doped *p*-type film, however, the optical loss initially increases due to the emergence of hole plasmonic behavior, followed by additional contributions from phonon−polariton interactions.

and confinement at nanoscale dimensions within this spectral band. However, unlike plasmonic materials, where optical losses are dominated by free-carrier scattering, phonon polaritons benefit from intrinsically low losses due to the longer lifetimes of optical phonons.[19] This key distinction makes SPhPs highly attractive for mid-to-far-infrared applications requiring lower optical losses,[19] such as near-field radiative heat transfer,[22−25] on-chip photonics,[26] and IR optoelectronics.[27] Therefore, the ability to generate hole plasmon resonances, (S)/PhPs, and enable their coupling in a *p*-type polar semiconductor could offer a compelling additional pathway to tailor and enhance the optical response of materials.

Conventionally, when plasmons and phonon polaritons coexist within a similar spectral range, their electromagnetic near-fields can hybridize, giving rise to mixed or coupled plasmon−phonon polariton modes with properties distinct from either constituent.[28−30] Plasmon−phonon hybrid modes have been realized using heterogeneous interfaces, typically comprising a doped plasmonic layer coupled to a polar dielectric. In such systems, the coupling strength depends on tuning the plasmon resonance to the phonon frequency of the adjacent layer and on achieving strong spatial overlap between the modes. Alternatively, a single host material that simultaneously supports free carriers and polar lattice vibrations within a similar spectral range provides a conceptually simpler platform for polaritonic hybridization. Such coupling has been extensively studied in the context of longitudinal optical phonon−plasmon coupling (LOPC) in polar *n*-type semiconductors.[30,31] Extending these concepts to *p*-type polar semiconductors, especially in the mid-to-far-infrared regime, represents a comparatively less explored direction. Demonstrating hole plasmon− LO-phonon mixing within a single host material thus provides a platform for tunable polaritonic responses in integrated photonic architectures.

Scandium nitride (ScN),[32−34] a refractory group III(B) transition metal nitride semiconductor, crystallizes in a cubic rocksalt structure with octahedral bonding coordination and offers a potential material platform to realize the hole plasmon and mixed plasmon-phonon modes.[35] ScN possesses an indirect bandgap of 0.9 eV and a direct bandgap of 2.2 eV.[34,36,37] Recognized for its outstanding mechanical hardness (∼21−23 GPa), corrosion resistance, and high melting temperature exceeding 2873 K, ScN has attracted considerable interest for use in thermoelectric energy conversion,[38−40] epitaxial semiconductor superlattices,[41−43] artificial synapses,[44] and Schottky diodes.[45] ScN thin films, typically grown via

https://doi.org/10.1021/acs.nanolett.6c02445
Nano Lett. 2026, 26, 9614−9621

molecular beam epitaxy (MBE) or magnetron sputtering, exhibit a high *n*-type carrier concentration in the 10^{20}–10^{21} cm^{-3} range mainly due to oxygen impurities, and a moderately high electron mobility (~60–120 cm^2 V^{-1} s^{-1}) at room-temperature.[33,38,46] Such high carrier concentrations shift the Fermi energy (E_F) ~ 0.2–0.3 eV inside the conduction band of ScN (Figure 1b), and results in tunable plasmonic behavior in the near-infrared spectral range (1–2.5 μm, or 10,000–4000 cm^{-1}).

Mg-acceptor doping has been used successfully for ScN, compensating for its high electron concentration and leading to *p*-type ScN with high hole concentrations (~2.2 × 10^{20} cm^{-3}) and mobility (~21 cm^2 V^{-1} s^{-1}).[47,48] Further, due to the polar bonds, a highly reflective Reststrahlen band (27.85–14.77 μm, or 359–677 cm^{-1}) also exists, enabling SPhP modes within this spectral range in ScN.[35] Therefore, with a high hole concentration and a moderate hole effective mass (0.8 m_e), ScN offers a promising candidate for exploring hole plasmon resonances near phonon frequencies, facilitating hole plasmon-phonon polariton *mixing* within a single host medium. In this work, we show moderately damped hole plasmons in epitaxial *p*-type ScN films in the mid-infrared spectral range, aligning closely with its phonon spectrum. Additionally, by tuning the hole concentrations, we observe a mixing between hole plasmons and phonon polaritons, leading to a broad hybrid optical mode in the mid-to-far-infrared, establishing ScN as a promising platform for hole-driven infrared plasmonics and polariton-based light-matter interactions.

Intentionally undoped and Mg-hole-doped ScN thin films (Table 1) were deposited on (001) MgO substrates with an ultrahigh vacuum reactive magnetron sputtering at a base pressure of 1 × 10^{-9} Torr (see Section 1 in the Supporting Information (SI) for detailed growth method). Without intentional doping, as-deposited ScN is a *n*-type semiconductor exhibiting a high electron concentration of 3.3 × 10^{20} cm^{-3} and a moderate mobility of 43 cm^2/V·s at room-temperature. Such a high electron density in *n*-type ScN leads to a small increase in resistivity as a function of temperature (see Figure S2b in SI section 3.1), reminiscent of its degenerate electronic nature. Further, negative values of the Seebeck coefficient (Figure S2c) establishes its *n*-type carrier transport behavior.[38] However, with the incorporation of Mg-hole-doping, ScN undergoes an *n*-to-*p* carrier type transition, as the E_F moves close to the valence band with increasing hole concentration (Figure 1b).[47] Since substitutional magnesium on scandium (Mg_{Sc}) hole-dopants exhibits a very low activation energy, most dopants are ionized at room-temperature, causing a high hole concentration of 1.4 × 10^{20} cm^{-3} for the film with maximum hole dopants.[32,47] Like *n*-type ScN, *p*-type ScN films also exhibit a weak temperature dependence of resistivity and positive Seebeck coefficients due to holes as the energy carriers (see Figure S2 in SI section 3.1).

Table 1. Electrical Properties of ScN, Including Carrier Concentration, Mobility, and Resistivity

Sample Name	Sample Composition	Carrier concentration (cm^{-3})	Mobility (cm^2 V^{-1} s^{-1})	Resistivity (Ω cm)
n-type	Undoped ScN	3.3 × 10^{20}	43	4.4 × 10^{-4}
Low-doped *p*-type	ScN:Mg	1.6 × 10^{18}	1.2	3.6
Highly doped *p*-type	ScN:Mg	1.4 × 10^{20}	20	2.3 × 10^{-3}

The real component of the dielectric permittivity (ε') extracted from spectroscopic ellipsometry measurements extending across the near-UV to far-IR spectral range (see section 2.1 and 3.3 in SI for details), show that ε' remains positive in the near-UV–visible spectral region for all ScN films (Figure 1c and 1e), highlighting their dielectric nature. However, as the wavelength increases, ε' in *n*-type ScN undergoes a positive-to-negative permittivity transition in the near-infrared at ~4250 cm^{-1} (2.35 μm), highlighting the onset of its plasmonic response and epsilon-near-zero (ENZ) behavior. Such near-infrared ENZ response in *n*-type ScN is consistent with previous observations.[35] However, compared to the *n*-type film, ε' in highly doped *p*-type ScN undergoes an ENZ crossover at ~1200 cm^{-1} (8.33 μm) representing the onset of the plasmonic behavior (see inset in Figure 1e) in the mid-infrared spectral range. For low-doped *p*-type films with lower hole concentrations (see Table 1), the ENZ crossover shifts to even lower energies, falling outside the spectral regime accessible with ellipsometry measurements (above 250 cm^{-1} (40 μm)).

The positive-to-negative ε' crossover observed in highly doped *p*-type ScN provides clear evidence of a hole plasmon resonance, rather than the conventional plasmonic response driven by electronic oscillations. Such hole plasmon resonances in the mid-infrared region have previously been reported in *p*-type semiconductors, such as GaAs at low temperatures (~80 K) and with high-resolution electron energy loss spectroscopy measurements.[15] Low-temperature measurements were necessary because the low hole concentration in previously reported *p*-type GaAs resulted in a plasma frequency in the far-infrared range, where phonon-limited carrier damping, which increases further at room-temperature, was sufficient to substantially broaden the hole-plasmon resonance, making it difficult to resolve outside cryogenic conditions. In contrast, the much higher carrier concentration in ScN pushes the plasma frequency into the mid-IR, where the modest damping we observed was sufficiently low to allow room temperature observations of the hole-plasmon resonance. Although mid-infrared plasmonic responses have previously been demonstrated in doped *n*-type semiconductors such as CdO and InAs,[49,50] this work demonstrates the first observation of room-temperature hole plasmons in *p*-type ScN, marking a significant advancement in the field of plasmonics based on *p*-type semiconductors.

Beyond the plasmonic response, the polar nature of ScN ensures that all films exhibit phonon-polariton behavior (Figure 1e). The low-doped *p*-type film (see Table 1), shows a clear pole around the TO phonon frequency (359 cm^{-1}), signifying strong coupling of IR light with TO phonon vibrations. Consequently, the ε' becomes negative between the LO (677 cm^{-1}) and TO (359 cm^{-1}) phonon frequencies, forming the Reststrahlen band. Due to the low hole concentration and mobility, the low-doped *p*-type film lacks hole plasmonic behavior in the ellipsometry accessible spectral range and their dielectric response is governed solely by the phonon contributions as shown in the expression for total dielectric permittivity in eq 1.[35]

https://doi.org/10.1021/acs.nanolett.6c02445
Nano Lett. 2026, 26, 9614–9621

$$\varepsilon(\omega) = \varepsilon_1(\omega) + i\varepsilon_2(\omega) = \varepsilon_\infty\left(1 - \frac{\omega_p^2}{\omega^2 + i\omega\Gamma} + \frac{\omega_{LO}^2 - \omega_{TO}^2}{\omega_{TO}^2 - \omega^2 - i\omega\gamma}\right) \quad (1)$$

where $-\frac{\omega_p^2}{\omega^2 + i\omega\Gamma}$ and $\frac{\omega_{LO}^2 - \omega_{TO}^2}{\omega_{TO}^2 - \omega^2 - i\omega\gamma}$ represent charge carriers and phonon contributions to the overall dielectric permittivity, respectively, and the plasma frequency is defined as

$$\omega_p = \sqrt{\frac{n_c e^2}{m_c^* \varepsilon_0}} \quad (2)$$

Here, ε_∞, Γ, ω_{LO}, ω_{TO}, γ, n_c, m_c^*, ε_0, and e are the high-frequency dielectric constant, plasmon damping constant, LO and TO phonon frequencies, phonon damping constant, majority carrier concentration, carrier effective mass, permittivity of free space, and electronic charge, respectively. However, as the hole concentration increases, the hole plasma frequency rises, shifting the crossover to higher energies and the hole plasmon behavior dominates over the phonon-polariton effects, as evident in Figure 1e. In highly doped *p*-type ScN, the hole plasmonic behavior emerges at higher frequencies (1200 cm^{-1}), suppressing the phonon-polariton response, and ε' remains negative below the hole plasma frequency. For *n*-type ScN, as the plasmonic response is much stronger leading to its high $|\varepsilon'|$ values in the mid-to-far-infrared range, phonon-polariton behavior is weak, evidenced by the minimal changes in ε' at the TO phonon frequencies (Figure 1c). Notably, despite the nearly equal electron and hole concentrations in *n*-type and highly doped *p*-type samples, the spectral position of the plasmonic responses differs primarily due to the higher effective mass of holes ($0.8m_e$) compared to electrons ($0.39m_e$).

The imaginary component of the dielectric permittivity (ε''), representing optical losses, is observed as an absorption peak at ~17,700 cm^{-1} (560 nm) in all three films due to ScN's direct band gap transition. In the near-infrared region, optical losses are low for all films represented as low ε'' values in the 0.02−0.64 range at 5000 cm^{-1} (2 μm). However, *n*-type ScN, exhibiting plasmonic behavior at short-wavelength infrared region, shows an increase in the ε'' with decreasing wavelength due to the free electron Drude absorption (Figure 1d). Conversely, low-doped *p*-type ScN with low hole concentrations lacks the Drude absorption across the near-to-far-infrared spectral range but displays a prominent peak at the TO phonon frequency, due to the strong light-TO phonon coupling (Figure 1f). With the increase in Mg-doping, the hole concentration in highly doped *p*-type ScN film also increases, resulting in the hole plasmonic behavior dominating the dielectric function, causing the magnitude of ε'' to rise at longer wavelength and demonstrating a peak at the TO phonon frequency.

At the ENZ condition, the highly doped *p*-type ScN exhibits higher optical losses ($\varepsilon'' \approx 3.8$) than its *n*-type counterpart ($\varepsilon'' \approx 0.6-1.2$), consistent with the lower mobility and enhanced carrier damping associated with holes. Nevertheless, this loss remains comparatively low within the broader context of hole plasmonic materials, where *p*-type Si typically exhibit higher optical losses, with $\varepsilon'' \sim 6$.[51] Notably, propagating surface hole plasmon polariton in *p*-type ScN/air waveguides exhibit a calculated propagation length (L) of ~ 10.61 μm, confinement width (D) of ~4.6 μm and *figure of merit* (FOM = $\frac{L}{D}$) ~2.25 at the Fröhlich resonance condition ($\varepsilon' = -2$) (see Figure S8 in SI section 3.7), making it potentially suitable for efficient and compact plasmonic device integration across diverse applications, including waveguides, hyperbolic metamaterials (HMMs), and transformation optics.

The emergence of hole plasmon excitations in highly doped *p*-type ScN films in the mid-infrared spectral range opens the possibility of mixing hole plasmons with phonon polariton modes. To explore this, polarization-dependent ATR-FTIR measurements were carried out using a diamond crystal in a standard single-bounce attenuated total reflection geometry, as illustrated schematically in Figure 2a. The dispersion relations

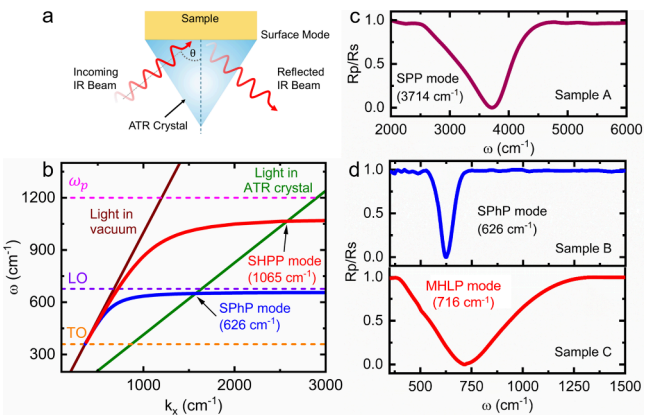

Figure 2. Surface phonon-polaritons and mixed hole plasmon-LO phonon mode in ScN. (a) Schematic representation of the attenuated total reflectance (ATR) measurement setup used to probe surface plasmon and phonon polariton resonances. (b) Calculated polariton dispersion curves, comparing the surface phonon polariton mode in low-doped *p*-type ScN with the hole plasmon polariton mode in highly doped *p*-type ScN. (c) Normalized ATR reflectance spectrum plotted as the ratio between the *p*-polarized to *s*-polarized light intensity of *n*-type ScN, exhibiting the excitation of a surface plasmon polariton mode at 3714 cm^{-1} (2.69 μm). (d) Normalized ATR reflectance spectrum plotted as the ratio between the *p*-polarized to *s*-polarized light intensity highlighting the excitation of the surface phonon polariton mode in low-doped *p*-type ScN at 626 cm^{-1} (15.97 μm) close to its LO phonon frequency. Compared to the low-doped ScN, the highly doped ScN film shows a broad mixed hole plasmon-LO phonon (MHLP) mode.

for the SPhP and surface hole plasmon polariton are calculated using the experimentally measured dielectric permittivity of low-doped and highly doped *p*-type ScN films and *n*-type ScN, respectively, providing theoretical validation of the polaritonic dispersion observed in the ATR measurements (Figure 2b and Figure S7 in SI section 3.5).

In the *n*-type ScN film, the polarization-dependent ATR spectrum exhibits a dip at 3714 cm^{-1} (2.69 μm), attributed to the excitation of the SPP mode (Figure 2c). The spectral position and full width at half-maximum (fwhm) of the peak width of 772 cm^{-1} are consistent with the previously reported SPP mode excitation in *n*-type ScN.[35] In the low-doped *p*-type ScN film, a dip in ATR reflectivity spectrum appears at 626 cm^{-1} (15.97 μm) due to the excitation of the SPhP mode, where the light line in diamond intersects the SPhP dispersion curve (Figure 2d). Notably, the ATR dip associated with the SPhP mode exhibits a significantly narrower fwhm of 63 cm^{-1}

https://doi.org/10.1021/acs.nanolett.6c02445
Nano Lett. 2026, 26, 9614−9621

compared to that of the SPP mode, reflecting the intrinsically longer lifetimes of SPhP excitations (see section 3.13 in SI).

For the highly doped *p*-type ScN film, the dispersion curve reveals that the light line in the diamond crystal crosses the hole plasmon polariton dispersion at 1065 cm^{-1} (9.38 μm). However, in the corresponding ATR spectrum, a broad dip centered at 716 cm^{-1} (13.96 μm) is detected. This hybrid optical mode arises from the mixing of the hole plasmon polariton (PP) and phonon polariton (PhP) modes in the ScN film, referred to as the mixed hole-plasmon−LO-phonon optical response. Notably, the peak position of this mode occurs at a significantly shorter wavelength than both the SPhP mode of ScN at 626 cm^{-1} (15.97 μm) and the LO phonon frequency at 677 cm^{-1} (14.77 μm). Moreover, the line width of this mixed mode is 342 cm^{-1}, lying between those of the SPP and SPhP modes, consistent with its mixed plasmon−phonon character. Thus, ATR measurements reveal a pronounced mixing between hole plasmon and phonon polariton modes within a single host material, ScN, paving the way for tunable polaritonic responses in the mid-to-long wavelength infrared regime using doped semiconductor platforms, which can be useful for sensing, thermal emission engineering, and mid-infrared photonic device applications.

The reflection spectra of the *p*-type ScN films are measured further using Fourier transform infrared (FTIR) spectroscopy. Owing to its polar dielectric character, ScN exhibits negative permittivity in the spectral region between the TO and LO phonon frequencies, resulting in exceptionally high reflectivity and the formation of the Reststrahlen band. As shown in Figure 3a, the Reststrahlen band of low-doped *p*-type ScN exhibits a rectangular shape, whereas the highly doped *p*-type ScN exhibits a trapezoidal shape due to the increased absorption of light from the LOPC effect. In highly doped *p*-type ScN, reflectivity decreases progressively from the TO phonon frequency at 359 cm^{-1} to the LO phonon frequency at 677 cm^{-1}, which further highlights the impact of the plasmon-phonon interactions.[52] The low-doped *p*-type ScN sample, with a hole concentration of 1.6 × 10^{18} cm^{-3}, shows a negligible plasmonic contribution to the dielectric permittivity in the mid-to-far-infrared spectral range, resulting in a pronounced phonon-polaritonic response, as confirmed from the dielectric permittivity spectra (Figure 1e). In contrast, the high-doped *p*-type ScN, with a hole concentration of 1.4 × 10^{20} cm^{-3}, exhibits a significant hole-plasmon contribution to the dielectric permittivity. Consequently, the Reststrahlen band acquires a tapered shape due to the softening of the high frequency edge, consistent with the reflectivity profile theoretically predicted using Fresnel's equations and validated by the experimental reflection data (see section 3.12 in SM for details).

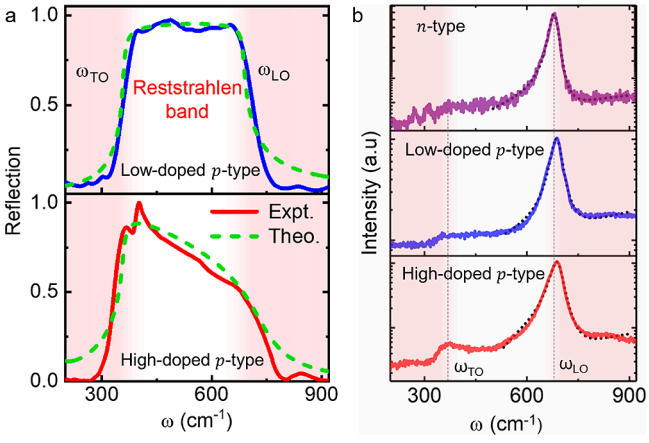

Figure 3. Evolution of the Reststrahlen band and Raman spectra in *p*-type ScN films. (a) Reststrahlen bands of low-doped and highly doped *p*-type ScN films, exhibiting rectangular and trapezoidal shape profiles, respectively. The trapezoidal shape observed in the highly doped *p*-type ScN arises from the increased absorption of light from the mixed hole-plasmon phonon polariton mode as discussed above. The rectangular-to-trapezoidal shape change of the Reststrahlen band in *p*-type ScN provide further evidence of the plasmon-phonon mixing. (b) Raman spectra of the three ScN films, showing the presence of LO phonon modes, while TO modes appear in the highly doped *p*-type ScN. The Raman spectra were fitted with Fano profile around the asymmetric LO phonon frequency to highlight the carrier (hole)-phonon interactions. The increase in the LO phonon frequency in highly doped ScN originates from a wavevector-dependent Raman scattering involving mixed hole−plasmon LO phonon mode.

The optical phonon frequencies of *n*-type and *p*-type ScN films are further investigated using Raman spectroscopy, as shown in Figure 3b. Owing to the cubic rocksalt crystal structure of ScN, first-order Raman scattering is symmetry forbidden. However, the presence of defects relaxes the momentum (q) selection rules, enabling the detection of phonon modes. The *n*-type ScN film exhibits a prominent Raman peak at 676.2 cm^{-1}, corresponding to the LOPC mode, in agreement with earlier reports.[52,53] Similarly, the *p*-type ScN films display well-defined phonon modes, with frequencies 686.2 cm^{-1} and 686.9 cm^{-1} for the low-doped and highly doped samples, respectively. The slight upward shift in the phonon frequency can be attributed to wavevector-dependent Raman scattering involving LOPC modes, previously observed in *n*-type ScN with varying electron concentrations.[52] In addition, a weak feature appears near 359 cm^{-1} in the highly doped *p*-type films, which is assigned to the TO phonon mode of ScN.

The Raman modes exhibit an asymmetric line-shape, characteristic of Fano resonance, arising from the interaction between the discrete phonon mode and a continuum of charge carrier excitations. In highly doped *p*-type ScN, where the hole concentration exceeds 1 × 10^{20} cm^{-3}, the Fermi level shifts into the valence band, giving rise to an electronic excitation continuum that overlaps in energy with the LO phonon. The resulting interference between these discrete and continuum states leads to the observed Fano-type asymmetry, consistent with the behavior reported in heavily doped *n*-type ScN,[52] as well as several other semiconductor materials.[54] The LO phonon Raman mode line-shape was fitted using a Fano profile, yielding the Fano asymmetry parameter values from 6.8 to 13.2 and resonance-width parameter of 19−20 cm^{-1} (see section 3.6 in SI) for the three films.

The optical response discussed above, particularly the emergence and characteristics of the hole plasmon resonance, critically depends on the crystalline quality, dopant incorporation, and microstructural uniformity of the Mg-doped ScN films. To establish this structure−property relationship, the microstructure of the Mg hole-doped ScN thin films was investigated using high-resolution X-ray diffraction (HRXRD) and transmission electron microscopy (TEM). While detailed structural characterization of Mg-doped ScN has been reported previously,[47] all three films examined in this study exhibit a

https://doi.org/10.1021/acs.nanolett.6c02445
Nano Lett. 2026, 26, 9614−9621

(002) preferred orientation on (001) MgO substrates, as confirmed by HRXRD (see section 3.14 in SI).

To further elucidate the microstructure of the highly doped *p*-type ScN film, high-angle annular dark-field scanning transmission electron microscopy (HAADF-STEM), energy-dispersive X-ray spectroscopy (EDS) mapping, and electron diffraction analyses were performed. The Mg-doped ScN films, deposited on (001) MgO substrates at elevated temperatures, exhibit epitaxial growth with a well-defined cube-on-cube crystallographic relationship of ScN (001)[001]||(001)[001] MgO (Figures 4a and 4b). Despite the ~7% lattice mismatch

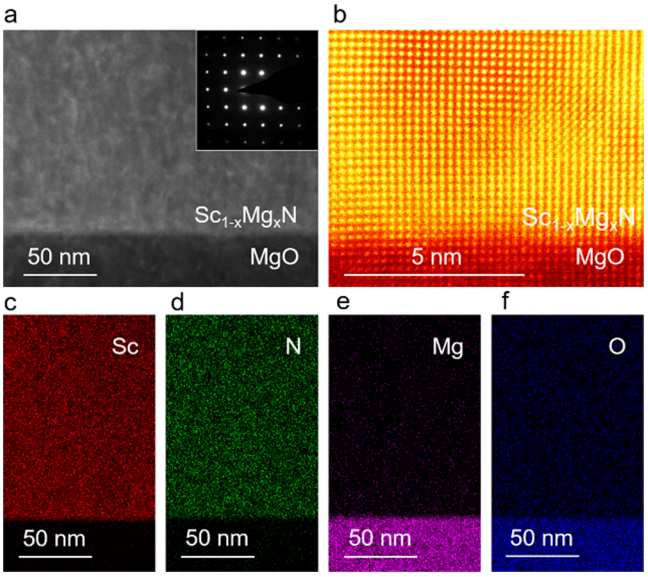

Figure 4. Microstructural characterizations of highly doped *p*-type ScN film. (a) Low-magnification HAADF-STEM image illustrating uniform and homogeneous Mg-hole doped ScN film. The inset displays the selected area electron diffraction (SAED) pattern, confirming cubic epitaxial growth. The microscopy imaging was performed along the [001] zone axis. (b) Atomic-resolution STEM image of the $Sc_{1-x}Mg_xN$/MgO interface, revealing a sharp interface and cube-on-cube epitaxial alignment. (c–f) STEM-EDS elemental maps showing the spatial distribution of (c) Sc, (d) N, (e) Mg, and (f) O, indicating a uniform elemental composition across the film.

between ScN and MgO, the interface remains sharp, with only a limited density of misfit dislocations. Notably, both oxygen and magnesium dopants are uniformly incorporated into the ScN matrix, forming homogeneous solid solutions without any evidence of precipitation or secondary phase formation, as confirmed by the EDS elemental maps (Figures 4c–f). Such uniform dopant distribution and high crystalline quality are consistent with the moderate plasmon damping and well-defined optical response observed in these films.

In summary, we report the experimental realization of low-loss, high-quality room-temperature hole plasmons and their mixing with phonon polaritons in epitaxial refractory group-III polar *p*-type semiconductor ScN, operating in the mid-infrared regime. This plasmonic response is driven by a high hole concentration of 1.4×10^{20} cm^{-3} and notable hole mobility of 21 cm^2 V^{-1} s^{-1} at room-temperature. Through prism-coupling measurements, we reveal a pronounced hybridization between the hole plasmons and LO-phonon, resulting in a broad, hybrid mode, the mixed hole-plasmon − LO-phonon optical response. The realization of tunable, hole-driven plasmon−phonon hybrid modes in epitaxial ScN establishes a new material platform for infrared polaritonics, complementing prior studies in conventional polar semiconductors. These findings position ScN as a highly promising platform for integrated, low-loss, and tunable polaritonic devices, with potential impact across waveguiding, hole-driven plasmonics, infrared optoelectronics, and thermal photonic technologies.

■ ASSOCIATED CONTENT

Data Availability Statement

The data that support the findings of this study are available from the corresponding author upon reasonable request.

Supporting Information

See the Supporting Information for . The Supporting Information is available free of charge at https://pubs.acs.org/doi/10.1021/acs.nanolett.6c02445.

Growth, characterization, and ellipsometry measurements and data fitting analysis (PDF)

■ AUTHOR INFORMATION

Corresponding Author

Bivas Saha − *Chemistry and Physics of Materials Unit, Jawaharlal Nehru Centre for Advanced Scientific Research, Bangalore 560064, India; International Centre for Materials Science and School of Advanced Materials, Jawaharlal Nehru Centre for Advanced Scientific Research, Bangalore 560064, India;* orcid.org/0000-0002-0837-1506; Email: bsaha@jncasr.ac.in, bivas.mat@gmail.com

Authors

Prasanna Das − *Chemistry and Physics of Materials Unit, Jawaharlal Nehru Centre for Advanced Scientific Research, Bangalore 560064, India; International Centre for Materials Science, Jawaharlal Nehru Centre for Advanced Scientific Research, Bangalore 560064, India;* orcid.org/0000-0003-1138-7557

Debmalya Mukhopadhyay − *Chemistry and Physics of Materials Unit, Jawaharlal Nehru Centre for Advanced Scientific Research, Bangalore 560064, India; International Centre for Materials Science, Jawaharlal Nehru Centre for Advanced Scientific Research, Bangalore 560064, India*

Emma R. Bartelsen − *Interdisciplinary Materials Science Program, Vanderbilt University, Nashville, Tennessee 37212, United States;* orcid.org/0009-0005-0369-0750

Renuka Karanje − *Chemistry and Physics of Materials Unit, Jawaharlal Nehru Centre for Advanced Scientific Research, Bangalore 560064, India; International Centre for Materials Science, Jawaharlal Nehru Centre for Advanced Scientific Research, Bangalore 560064, India*

Krishna Chand Maurya − *Chemistry and Physics of Materials Unit, Jawaharlal Nehru Centre for Advanced Scientific Research, Bangalore 560064, India; International Centre for Materials Science, Jawaharlal Nehru Centre for Advanced Scientific Research, Bangalore 560064, India*

Pavithra Rao − *Centre for Nano Science and Engineering (CeNSE), Indian Institute of Science, Bangalore 560012, India*

Ashalatha Indiradevi Kamalasanan Pillai − *Sydney Microscopy and Microanalysis, The University of Sydney, Camperdown, New South Wales 2006, Australia*

https://doi.org/10.1021/acs.nanolett.6c02445
Nano Lett. 2026, 26, 9614−9621

Shankar Kumar Selvaraja − *Centre for Nano Science and Engineering (CeNSE), Indian Institute of Science, Bangalore 560012, India*

Magnus Garbrecht − *Sydney Microscopy and Microanalysis, The University of Sydney, Camperdown, New South Wales 2006, Australia;* orcid.org/0000-0002-1852-5580

Joshua D. Caldwell − *Interdisciplinary Materials Science Program, Vanderbilt University, Nashville, Tennessee 37212, United States; Department of Mechanical Engineering, Vanderbilt University, Nashville, Tennessee 37212, United States;* orcid.org/0000-0003-0374-2168

Complete contact information is available at: https://pubs.acs.org/10.1021/acs.nanolett.6c02445

Author Contributions

P.D., D.M., and E.R.B. contributed equally to this work. B.S. conceived this project. P.D., D.M., E.R.B., and P.R. performed the optical characterizations. R.K. and K.C.M. deposited thin films. R.K. performed the Seebeck coefficient and electrical transport measurements. A.I.K.P. performed TEM sample preparation. M.G. performed TEM imaging and EDS mapping. S.K.S., J.D.C., and B.S. contributed to the discussion and interpretation of the results. All authors discussed and contributed to the preparation of the manuscript.

Notes

The authors declare no competing financial interest.

■ ACKNOWLEDGMENTS

B.S. acknowledges the International Centre for Materials Science and Sheikh Saqr Laboratory of Jawaharlal Nehru Centre for Advanced Scientific Research for support. B.S. acknowledges the Anusandhan National Research Foundation in India for a Core Research Grant No. CRG/2023/007061 for financial support. P.D. thanks the Council of Scientific & Industrial Research for the fellowship. P.D. thanks Sourav Rudra and Dheemahi Rao for their help in calculating band structure and helping in Seebeck coefficient measurement. *The authors acknowledge the SAMat Research Facilities, JNCASR, Bengaluru.* J.D.C. was supported by the Office of Naval Research (ONR) under Grant No. N00014-22-1-2035, E.R.B. was supported by the Vanderbilt Innovation Catalyst Grant. M.G. and A.I.K.P. acknowledge the Sydney Microscopy and Microanalysis facilities at the University of Sydney.

■ REFERENCES

(1) Maier, S. A.; Brongersma, M. L.; Kik, P. G.; Meltzer, S.; Requicha, A. A. G.; Atwater, H. A. Plasmonics - A Route to Nanoscale Optical Devices. *Adv. Mater.* **2001**, *13* (19), 1501−1505.

(2) Schuller, J. A.; Barnard, E. S.; Cai, W.; Jun, Y. C.; White, J. S.; Brongersma, M. L. Plasmonics for Extreme Light Concentration and Manipulation. *Nat. Mater.* **2010**, *9* (3), 193−204.

(3) Basov, D. N.; Fogler, M. M.; García De Abajo, F. J. Polaritons in van Der Waals Materials. *Science* **2016**, *354* (6309), aag1992.

(4) Folland, T. G.; Nordin, L.; Wasserman, D.; Caldwell, J. D. Probing Polaritons in the Mid- to Far-Infrared. *J. Appl. Phys.* **2019**, *125* (19), 191102.

(5) Zayats, A. V.; Smolyaninov, I. I.; Maradudin, A. A. Nano-Optics of Surface Plasmon Polaritons. *Phys. Rep.* **2005**, *408* (3−4), 131−314.

(6) Dunkelberger, A. D.; Ellis, C. T.; Ratchford, D. C.; Giles, A. J.; Kim, M.; Kim, C. S.; Spann, B. T.; Vurgaftman, I.; Tischler, J. G.; Long, J. P.; Glembocki, O. J.; Owrutsky, J. C.; Caldwell, J. D. Active Tuning of Surface Phonon Polariton Resonances via Carrier Photoinjection. *Nat. Photonics* **2018**, *12* (1), 50−56.

(7) Naik, G. V.; Shalaev, V. M.; Boltasseva, A. Alternative Plasmonic Materials: Beyond Gold and Silver. *Adv. Mater.* **2013**, *25* (24), 3264−3294.

(8) Exarhos, G. J.; Zhou, X. D. Discovery-Based Design of Transparent Conducting Oxide Films. *Thin Solid Films* **2007**, *515* (18), 7025−7052.

(9) Stewart, M. E.; Anderton, C. R.; Thompson, L. B.; Maria, J.; Gray, S. K.; Rogers, J. A.; Nuzzo, R. G. Nanostructured Plasmonic Sensors. *Chem. Rev.* **2008**, *108* (2), 494−521.

(10) Truong, H.; Hoang, T.; Chung, K.; Lee, L. P. Plasmonic Biosensors and Actuators for Integrated Point-of-Care Diagnostics. *npj Biosensing* **2025**, *2* (1), 45.

(11) Ye, W.; Long, R.; Huang, H.; Xiong, Y. Plasmonic Nanostructures in Solar Energy Conversion. *J. Mater. Chem. C* **2017**, *5* (5), 1008−1021.

(12) Noginov, M. A.; Gu, L.; Livenere, J.; Zhu, G.; Pradhan, A. K.; Mundle, R.; Bahoura, M.; Barnakov, Y. A.; Podolskiy, V. A. Transparent Conductive Oxides: Plasmonic Materials for Telecom Wavelengths. *Appl. Phys. Lett.* **2011**, *99* (2), 021101.

(13) Willets, K. A.; Wilson, A. J.; Sundaresan, V.; Joshi, P. B. Super-Resolution Imaging and Plasmonics. *Chem. Rev.* **2017**, *117* (11), 7538−7582.

(14) You, X.; Fan, Z.; Zhang, H.; Xie, Z.; Li, C.; Gui, H.; Zou, G.; Zhan, Q.; Liu, J.; Liu, X.; Zhang, D. Large Field-of-View Plasmonic Scattering Imaging and Sensing of Nanoparticles with Isotropic Point-Spread-Function. *Nat. Commun.* **2025**, *16* (1), 1−11.

(15) Meng, Y.; Anderson, J. R.; Hermanson, J. C.; Lapeyre, G. J. Hole Plasmon Excitations on a p -Type GaAs(110) Surface. *Phys. Rev. B* **1991**, *44* (8), 4040−4043.

(16) Fukasawa, R.; Perkowitz, S. Raman-Scattering Spectra of Coupled LO-Phonon-Hole-Plasmon Modes in p -Type GaAs. *Phys. Rev. B* **1994**, *50* (19), 14119−14124.

(17) Du, G.; Zhao, L.; Li, S.; Huang, J.; Fang, S.; Han, W.; Li, J.; Du, Y.; Ming, J.; Zhang, T.; Zhang, J.; Kang, J.; Li, X.; Xu, W.; Chen, Y. Interlayer Engineering of Lattice Dynamics and Elastic Constants of 2D Layered Nanomaterials under Pressure. *Nat. Commun.* **2025**, *16*, 4−12.

(18) Han, W.; Feng, J.; Dong, H.; Cheng, M.; Yang, L.; Yu, Y.; Du, G.; Li, J.; Du, Y.; Zhang, T.; Wang, Z.; Chen, B.; Shi, J.; Chen, Y. Pressure-Modulated Structural and Magnetic Phase Transitions in Two-Dimensional FeTe: Tetragonal and Hexagonal Polymorphs. *Nano Lett.* **2024**, *24*, 966.

(19) Caldwell, J. D.; Lindsay, L.; Giannini, V.; Vurgaftman, I.; Reinecke, T. L.; Maier, S. A.; Glembocki, O. J. Low-Loss, Infrared and Terahertz Nanophotonics Using Surface Phonon Polaritons. *Nanophotonics* **2014**, *4* (1), 44−68.

(20) Barra-Burillo, M.; Muniain, U.; Catalano, S.; Autore, M.; Casanova, F.; Hueso, L. E.; Aizpurua, J.; Esteban, R.; Hillenbrand, R. Microcavity Phonon Polaritons from the Weak to the Ultrastrong Phonon-Photon Coupling Regime. *Nat. Commun.* **2021**, *12* (1), 1−9.

(21) Spann, B. T.; Compton, R.; Ratchford, D.; Long, J. P.; Dunkelberger, A. D.; Klein, P. B.; Giles, A. J.; Caldwell, J. D.; Owrutsky, J. C. Photoinduced Tunability of the Reststrahlen Band in 4H-SiC. *Phys. Rev. B* **2016**, *93* (8), 1−6.

(22) Song, B.; Ganjeh, Y.; Sadat, S.; Thompson, D.; Fiorino, A.; Fernández-Hurtado, V.; Feist, J.; Garcia-Vidal, F. J.; Cuevas, J. C.; Reddy, P.; Meyhofer, E. Enhancement of Near-Field Radiative Heat Transfer Using Polar Dielectric Thin Films. *Nat. Nanotechnol.* **2015**, *10* (3), 253−258.

(23) Li, D.; Pan, Z.; Caldwell, J. D. Phonon Polariton-Mediated Heat Conduction: Perspectives from Recent Progress. *J. Mater. Res.* **2024**, *39* (23), 3193−3201.

(24) Hutchins, W.; Zare, S.; Hirt, D. M.; Tomko, J. A.; Matson, J. R.; Diaz-Granados, K.; Long, M.; He, M.; Pfeifer, T.; Li, J.; Edgar, J. H.; Maria, J. P.; Caldwell, J. D.; Hopkins, P. E. Ultrafast Evanescent Heat Transfer across Solid Interfaces via Hyperbolic Phonon-Polariton Modes in Hexagonal Boron Nitride. *Nat. Mater.* **2025**, *24* (5), 698−706.

(25) Pan, Z.; Lu, G.; Li, X.; McBride, J. R.; Juneja, R.; Long, M.; Lindsay, L.; Caldwell, J. D.; Li, D. Remarkable Heat Conduction Mediated by Non-Equilibrium Phonon Polaritons. *Nature* **2023**, *623* (7986), 307−312.
(26) Xiong, H.; Lu, Y.; Wu, Q.; Li, Z.; Qi, J.; Xu, X.; Ma, R.; Xu, J. Topological Valley Transport of Terahertz Phonon-Polaritons in a $LiNbO_3$ Chip. *ACS Photonics* **2021**, *8* (9), 2737−2745.
(27) Gubbin, C. R.; De Liberato, S.; Folland, T. G. Surface Phonon Polaritons for Infrared Optoelectronics. *J. Appl. Phys.* **2022**, *131* (3), 030901.
(28) Qu, S.; Liu, H.; Dong, L.; Wu, L.; Ma, C.; Wang, S. Graphene-Hexagonal Boron Nitride Heterostructure as a Tunable Phonon-Plasmon Coupling System. *Crystals* **2017**, *7*, 49.
(29) Yoo, D.; de León-Pérez, F.; Pelton, M.; Lee, I. H.; Mohr, D. A.; Raschke, M. B.; Caldwell, J. D.; Martín-Moreno, L.; Oh, S. H. Ultrastrong Plasmon-Phonon Coupling via Epsilon-near-Zero Nanocavities. *Nat. Photonics* **2021**, *15* (2), 125−130.
(30) Woessner, A.; Lundeberg, M. B.; Gao, Y.; Principi, A.; Alonso-González, P.; Carrega, M.; Watanabe, K.; Taniguchi, T.; Vignale, G.; Polini, M.; Hone, J.; Hillenbrand, R.; Koppens, F. H. L. Highly Confined Low-Loss Plasmons in Graphene-Boron Nitride Heterostructures. *Nat. Mater.* **2015**, *14*, 421−425.
(31) Ortiga-Fibla, J.; Brunner, F.; Treidel, E. B.; Hilt, O.; Brusaterra, E.; Cros, A. Phonon-plasmon coupled modes in GaN vertical power structures: Carrier concentration and mobility analysis. *J. Appl. Phys.* **2025**, *138*, 045703.
(32) Biswas, B.; Saha, B. Development of Semiconducting ScN. *Phys. Rev. Mater.* **2019**, *3* (2), 1−25.
(33) Al-Atabi, H.; Zheng, Q.; Cetnar, J. S.; Look, D.; Cahill, D. G.; Edgar, J. H. Properties of Bulk Scandium Nitride Crystals Grown by Physical Vapor Transport. *Appl. Phys. Lett.* **2020**, *116* (13), 132103.
(34) Gall, D.; Städele, M.; Järrendahl, K.; Petrov, I.; Desjardins, P.; Haasch, R. T.; Lee, T. Y.; Greene, J. E. Electronic Structure of ScN Determined Using Optical Spectroscopy, Photoemission, and Ab Initio Calculations. *Phys. Rev. B - Condens. Matter Mater. Phys.* **2001**, *63* (12), 1251191−1251199.
(35) Maurya, K. C.; Rao, D.; Acharya, S.; Rao, P.; Pillai, A. I. K.; Selvaraja, S. K.; Garbrecht, M.; Saha, B. Polar Semiconducting Scandium Nitride as an Infrared Plasmon and Phonon-Polaritonic Material. *Nano Lett.* **2022**, *22* (13), 5182−5190.
(36) Deng, R.; Ozsdolay, B. D.; Zheng, P. Y.; Khare, S. V.; Gall, D. Optical and Transport Measurement and First-Principles Determination of the ScN Band Gap. *Phys. Rev. B - Condens. Matter Mater. Phys.* **2015**, *91* (4), 1−12.
(37) Al-Atabi, H. A.; Zhang, X.; He, S.; Chen, C.; Chen, Y.; Rotenberg, E.; Edgar, J. H. Lattice and Electronic Structure of ScN Observed by Angle-Resolved Photoemission Spectroscopy Measurements. *Appl. Phys. Lett.* **2022**, *121* (18), 182102.
(38) Rao, D.; Biswas, B.; Flores, E.; Chatterjee, A.; Garbrecht, M.; Koh, Y. R.; Bhatia, V.; Pillai, A. I. K.; Hopkins, P. E.; Martin-Gonzalez, M.; Saha, B. High Mobility and High Thermoelectric Power Factor in Epitaxial ScN Thin Films Deposited with Plasma-Assisted Molecular Beam Epitaxy. *Appl. Phys. Lett.* **2020**, *116* (15), 152103.
(39) Kerdsongpanya, S.; Van Nong, N.; Pryds, N.; Žukauskaite, A.; Jensen, J.; Birch, J.; Lu, J.; Hultman, L.; Wingqvist, G.; Eklund, P. Anomalously High Thermoelectric Power Factor in Epitaxial ScN Thin Films. *Appl. Phys. Lett.* **2011**, *99* (23), 232113.
(40) Bouteiller, H.; Burcea, R.; Poterie, C.; Fournier, D.; Giovannelli, F.; Nyman, J.; Ezzahri, Y.; Dubois, S.; Eklund, P.; le Febvrier, A.; Barbot, J. F. Improving the Thermoelectric Performance of Scandium Nitride Thin Films by Implanting Helium Ions. *Commun. Mater.* **2025**, *6* (1), 1−11.
(41) John, P.; Trampert, A.; Van Dinh, D.; Spallek, D.; Lähnemann, J.; Kaganer, V. M.; Geelhaar, L.; Brandt, O.; Auzelle, T. ScN/GaN(1100): A New Platform for the Epitaxy of Twin-Free Metal-Semiconductor Heterostructures. *Nano Lett.* **2024**, *24* (21), 6233−6239.
(42) Das, P.; Maurya, K. C.; Schroeder, J. L.; Garbrecht, M.; Saha, B. Near-UV-to-Near-IR Hyperbolic Photonic Dispersion in Epitaxial (Hf,Zr)N/ScN Metal/Dielectric Superlattices. *ACS Appl. Energy Mater.* **2022**, *5* (4), 3898−3904.
(43) Zhang, R.; Lin, T.; Peng, S.; Bi, J.; Zhang, S.; Su, G.; Sun, J.; Gao, J.; Cao, H.; Zhang, Q.; Gu, L.; Cao, Y. Flexible but Refractory Single-Crystalline Hyperbolic Metamaterials. *Nano Lett.* **2023**, *23* (9), 3879−3886.
(44) Rao, D.; Pillai, A. I. K.; Garbrecht, M.; Saha, B. Scandium Nitride as a Gateway III-Nitride Semiconductor for Both Excitatory and Inhibitory Optoelectronic Artificial Synaptic Devices. *Adv. Electron. Mater.* **2023**, *9* (3), 2200975.
(45) Rao, D.; Acharya, S.; Saha, B. Demonstration of Compensated n -Type Scandium Nitride Schottky Diodes. *J. Phys. D. Appl. Phys.* **2023**, *56* (7), 074004.
(46) Oshima, Y.; Villora, E. G.; Shimamura, K. Hydride Vapor Phase Epitaxy and Characterization of High-Quality ScN Epilayers. *J. Appl. Phys.* **2014**, *115* (15), 153508.
(47) Saha, B.; Garbrecht, M.; Perez-Taborda, J. A.; Fawey, M. H.; Koh, Y. R.; Shakouri, A.; Martin-Gonzalez, M.; Hultman, L.; Sands, T. D. Compensation of Native Donor Doping in ScN: Carrier Concentration Control and p-Type ScN. *Appl. Phys. Lett.* **2017**, *110* (25), 1−6.
(48) Rudra, S.; Rao, D.; Poncé, S.; Saha, B. Reversal of Band-Ordering Leads to High Hole Mobility in Strained p-Type Scandium Nitride. *Nano Lett.* **2023**, *23* (17), 8211−8217.
(49) Hwang, J. S.; Xu, J.; Raman, A. P. Simultaneous Control of Spectral And Directional Emissivity with Gradient Epsilon-Near-Zero InAs Photonic Structures. *Adv. Mater.* **2023**, *35*, 2302956.
(50) Nolen, J. R.; Runnerstrom, E. L.; Kelley, K. P.; Luk, T. S.; Folland, T. G.; Cleri, A.; Maria, J.-P.; Caldwell, J. D. Ultraviolet to Far-Infrared Dielectric Function of n -Doped Cadmium Oxide Thin Films. *Phys. Rev. Materials* **2020**, *4*, 025202.
(51) Shahzad, M.; Medhi, G.; Peale, R. E.; Tsuchikawa, R.; Ishigami, M.; Cleary, J.; Boreman, G. D.; Diaz, O. E. D. J.; Ted, A. Infrared Surface Waves on Semiconductor and Conducting Polymer. *Proc. SPIE* **2010**, *8024*, 1−8.
(52) Maurya, K. C.; Biswas, B.; Garbrecht, M.; Saha, B. Wave-Vector-Dependent Raman Scattering from Coupled Plasmon-Longitudinal Optical Phonon Modes and Fano Resonance in n-Type Scandium Nitride. *Phys. Status Solidi - Rapid Res. Lett.* **2019**, *13* (9), 1−6.
(53) Grümbel, J.; Goldhahn, R.; Feneberg, M.; Oshima, Y.; Dubroka, A.; Ramsteiner, M. Band Gaps and Phonons of Quasi-Bulk Rocksalt ScN. *Phys. Rev. Mater.* **2024**, *8*, L071601.
(54) Ma, B.; Jinno, D.; Miyake, H.; Hiramatsu, K.; Harima, H. Orientation Dependence of Polarized Raman Spectroscopy for Nonpolar, Semi-Polar, and Polar Bulk GaN Substrates. *Appl. Phys. Lett.* **2012**, *100*, 011909.

https://doi.org/10.1021/acs.nanolett.6c02445
Nano Lett. 2026, 26, 9614−9621